The 15th International Symposium on Magnetic Bearings, August 3-6, 2016, Mojiko Hotel, Kitakyushu, Japan

ISMB15

Torque interaction of the drive and active radial magnetic bearing in an ultra-high speed spinning ball motor

Marcel SCHUCK*, Daniel STEINERT** and Johann W. KOLAR*

* Power Electronic Systems Laboratory, Swiss Federal Institute of Technology
Technoparkstrasse 1, 8005 Zurich, Switzerland
E-mail: schuck@lem.ee.ethz.ch

** Levitronix GmbH
Technoparkstrasse 1, 8005 Zurich, Switzerland

Abstract

The ongoing miniaturization trend of electric machines increases the demand for higher rotational speeds to provide a required power level at decreased size. The goal of this project is to push the limits of rotor miniaturization by researching new concepts for ultra-high speed machines achieving rotational speeds above 20 million rotations per minute (Mrpm). Such high rotational speeds can only be attained by limiting the centrifugal loading on the rotor, which can be accomplished by decreasing its size to less than 1 mm in diameter. Furthermore, the rotational losses have to be minimized. This requires precise and fast frictionless magnetic bearings for stabilization of the rotor in all dimensions, which interfere with the drive system of the motor by generating a breaking torque and torque ripples. The interaction is studied in this paper based on an analytical model and transient finite element method (FEM) simulations. The occurring torque components are identified and guidelines for the design of the radial magnetic bearing are provided. By incorporating these guidelines into the machine design, acceleration of the rotor to the desired rotational speeds can be achieved.

Key words : Asynchronous machine, Magnetic bearing, Modeling and control, Spinning ball, Ultra-high speed

1. Introduction

The ongoing miniaturization trend of electric machines has led to increased rotational speeds in order to achieve high power densities. Small size drive systems with rotational speeds of up to 1 Mrpm have been developed in the past (Zwyssig, Kolar, and Round 2009). The achievable rotational speeds are limited by losses, which are mostly due to friction. Mechanical bearing friction can effectively be eliminated by using magnetic bearings. As air friction becomes significant at very high rotational speeds, it needs to be reduced by accelerating the rotor inside a vacuum. With a setup incorporating both aforementioned measures, rotational speeds exceeding 20 Mrpm have been achieved with a spherical steel rotor as early as 1946 (Beams, Young, and Moore 1946), but could not be reproduced in more recent studies (Boletis and Bleuler 2002, Boletis and Bleuler 2004). As the achievable rotational speed is ultimately limited by the tensile strength of the rotor material, sub-millimeter size solid steel spheres are used as rotors. At such scales, further limits are imposed by the controllability and precision of the employed magnetic bearing systems.

The goal of this project is to extend the limits of miniaturization with an ultra-high speed (UHS) motor reaching rotational speeds beyond 20 Mrpm. Ultimately, it is targeted at demonstrating the highest possible rotational speed with an electric motor. The conducted research helps to address existing challenges of conventional machines in regard to power density, mechanical stress and the controllability of highly dynamic systems. Moreover, the applicability of precise magnetic bearings for levitation and stabilization of rotors in the sub-millimeter range is demonstrated. The targeted ultra-high rotational speeds can be employed in applications such as gyroscopes, centrifuges and drilling devices, as well as in materials science research.

To achieve stable levitation of the rotor, the setup as shown in Fig. 1(a) is used, which implements an active magnetic bearing (AMB) in axial (z) and radial (x and y) direction based on an optical measurement of the rotor position in all dimensions. Due to the small geometries and space constraints around the rotor, a combined concept is used, in which the radially-placed drive coils are also used as radial bearing coils. During acceleration experiments it was observed that the radial AMB impairs the drive performance of the motor by having a decelerating effect. This paper presents a

concise analysis of this effect based on an analytical solution of the underlying electromagnetic field problem and provides guidelines for determining the admissible magnetic flux density magnitude ratios of the drive and bearing fields.

The remainder of this paper is organized as follows: Section 2 provides a brief description of the motor torque model and Section 3 considers the torque components as originating from the drive and bearing systems. The obtained results are verified through transient 3D FEM simulations in Section 4. Section 5 concludes the paper.

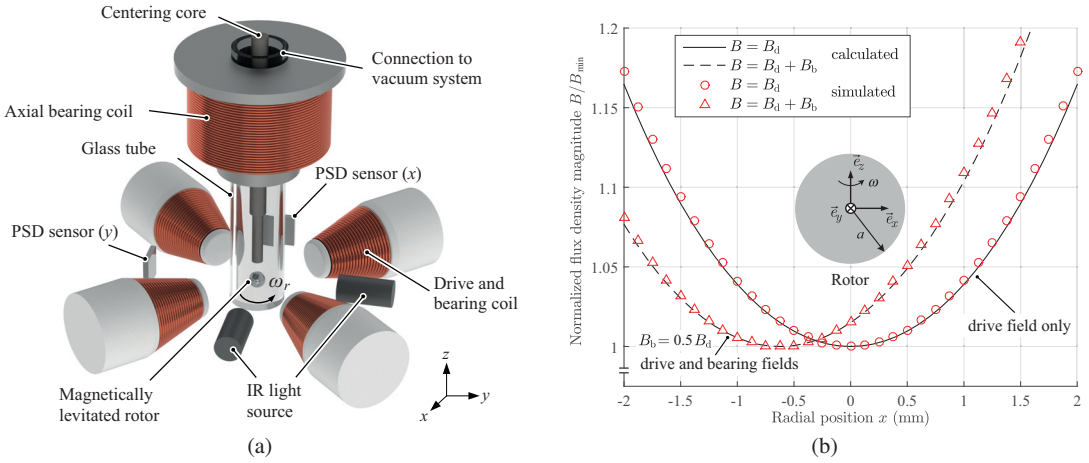

Fig. 1: Setup of the ultra-high speed motor with annotated components (a). Distribution of the magnetic flux density magnitude along the radial x-axis as caused by a drive field only ($B = B_d$) and a combined drive and bearing field ($B = B_d + B_b$), where B_b is generated by the coil in the positive x direction and its magnitude was chosen as $0.5B_d$ in the example (b). The flux density magnitude was normalized to its minimum value B_{min}, which occurs in the center of the motor for $B = B_d$ and is shifted for $B = B_d + B_b$ as shown. It can be seen that the simulation results are in good agreement with the calculated field distribution. More details regarding the utilized models are outlined in Section 4. A rotor of radius $a = 0.5$ mm including the relevant coordinate directions has been added to the figure.

2. Motor torque model

In order to study the interaction of the drive and radial bearing of the ultra-high speed spinning ball motor, the underlying mechanism of torque generation in the motor has to be known. Therefore, the corresponding model is briefly presented in this section.

The electromagnetic field problem of a rotating sphere made from conductive and ferromagnetic material in a rotating magnetic field with constant flux density magnitude has been solved in the work of Reichert, Nussbaumer, and Kolar 2012. As the rotor is accelerated by the principle of a solid rotor induction machine, it is subject to tangential Lorentz forces, which are generated due to the interaction of the eddy current density $\vec{J}$ inside the rotor and the rotating external magnetic flux density $\vec{B}$. The resulting torque is generally calculated by integrating over the volume of the spherical rotor as

$$\vec{T} = \int_0^{2\pi}\int_0^{\pi}\int_0^{a} \vec{r}\left(\vec{J}\times\vec{B}\right) r^2 \sin(\theta)\,\mathrm{d}r\,\mathrm{d}\theta\,\mathrm{d}\varphi, \tag{1}$$

where a denotes the rotor radius and $\vec{r}$ is the radius vector. This torque can alternatively be calculated via the magnetic dipole moment $\vec{m}$ of the sphere as caused by the magnitude B of the external magnetic flux density. The magnetic dipole moment $\vec{m}$ of a sphere is related to the magnetic vector potential $\vec{A}$ by

$$\vec{A} = \frac{\mu_0}{4\pi}\frac{\vec{m}\times\vec{r}}{r^3}, \tag{2}$$

see Jackson 1999. The magnetic vector potential $\vec{A}$ has been obtained by Reichert, Nussbaumer, and Kolar 2012 and is

used for the further considerations. By rearranging, $\vec{m}$ can be obtained as

$$\vec{m} = \begin{pmatrix} m_x \\ m_y \\ m_z \end{pmatrix} \approx \frac{2\pi}{\mu_0} a^3 \frac{B}{\sqrt{2} + \frac{p}{\sqrt{\omega_s}} + \frac{\sqrt{\omega_s}}{p}} \begin{pmatrix} \frac{3}{\sqrt{2}} + \frac{3p}{\sqrt{\omega_s}} \\ \frac{3}{\sqrt{2}} \\ 0 \end{pmatrix} \cdot \begin{pmatrix} \vec{e}_x \\ \vec{e}_y \\ \vec{e}_z \end{pmatrix} \quad \text{with} \quad p = \frac{1}{a}\sqrt{\frac{\mu_r}{\mu_0 \sigma}}, \tag{3}$$

where μ_r, σ, and ω_s denote the relative permeability of the rotor material, its conductivity, and the angular slip frequency, respectively. The latter is calculated as $\omega_s = \omega_f - \omega_r$, where ω_f is the angular frequency of the rotating magnetic field and ω_r is the angular frequency of the mechanical rotation of the sphere. The approximation in Eq. (3) results from a simplification of the magnetic vector potential $\vec{A}$, which has to be made in order to provide an analytic expression that allows to directly assess the dependency of the result on material parameters, rotor size, and operating conditions. The approximation yields sufficiently accurate results over a wide range of typical operating conditions and has implicitly also been used in Reichert, Nussbaumer, and Kolar 2012. By using the magnetic moment, the motor torque is obtained more explicitly than in Eq. (1) as

$$\vec{T} = \vec{m} \times \vec{B} = -B m_y \vec{e}_z. \tag{4}$$

3. Torque interaction of the drive and radial magnetic bearing

Based on the outlined model, it is now possible to study the interaction of the drive and radial AMB in the motor. The distribution of the magnetic flux density magnitude as present in the motor for a pure drive field as well as a combined drive and bearing field is shown in Fig. 1(b). The relevant vectors of the magnetic moments and flux densities are qualitatively shown in Fig. 2(a).

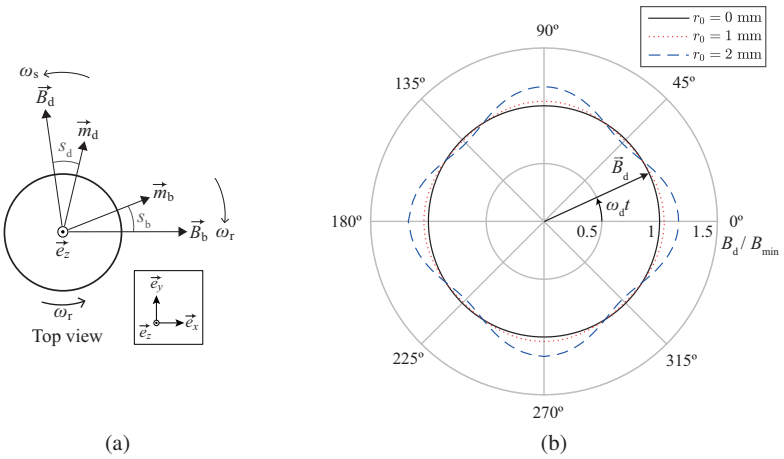

(a) (b)

Fig. 2: Flux density components and magnetic dipole moments as generated by the drive system and radial magnetic bearing in a rotor-oriented (rotating) coordinate system (a). Magnitude of the magnetic flux density at the center of the rotor for different displacements r_0 of the rotor from its equilibrium position at the center of the motor in a stator-oriented coordinate system (b). The shown values have been normalized to $B_d = B_{min}$, which occurs if the rotor is not displaced. The displayed circular shapes correspond to the trace as inscribed by the tip of the rotating flux density vector $\vec{B}_d$.

The magnetic flux density as generated by the drive is denoted by $\vec{B}_d$ and causes the magnetic moment $\vec{m}_d$. Both vectors rotate counterclockwise with an angular frequency of $\omega_f = \omega_d$ in a stator-oriented coordinate system and are rotated by the slip angle s_d with respect to one another. The latter can be calculated based on Eq. (3) as

$$s_d = \arctan\left(\frac{|m_{d,y}|}{|m_{d,x}|}\right) = \arctan\left(\frac{\sqrt{\omega_s}}{\sqrt{\omega_s} + \sqrt{2}p}\right). \tag{5}$$

As the rotor starts spinning with angular mechanical frequency ω_r, the rotational frequency of the two aforementioned vectors with respect to the rotor, which is relevant for the generation of the drive torque, is decreased to $\omega_s = \omega_d - \omega_r$, which will affect s_d as outlined in Eq. (5).

Additionally, the magnetic flux density $\vec{B}_\mathrm{b}$, as generated by the radial AMB, is stationary in a stator-oriented coordinate system ($\omega_\mathrm{f} = 0$), but rotates with ω_r in clockwise direction relative to the rotor. It causes the magnetic moment $\vec{m}_\mathrm{b}$, which is rotated by s_b with respect to $\vec{B}_\mathrm{b}$. In the depiction, $\vec{B}_\mathrm{b}$ has arbitrarily been chosen to point into the positive x direction.

Based on the model of Section 2, the desired accelerating drive torque with non-zero average value can be calculated as

$$\vec{T}_\mathrm{d} = -B_\mathrm{d} m_{\mathrm{d},y} \vec{e}_z \qquad \text{with} \quad \omega_\mathrm{s} = \omega_\mathrm{d} - \omega_\mathrm{r} \text{ in Eq. (3).} \tag{6}$$

The undesired breaking torque $\vec{T}_\mathrm{b}$, as generated by the radial AMB, can equivalently be calculated as

$$\vec{T}_\mathrm{b} = B_\mathrm{b} m_{\mathrm{b},y} \vec{e}_z \qquad \text{with} \quad \omega_\mathrm{s} = \omega_\mathrm{r} \text{ in Eq. (3).} \tag{7}$$

It should be noted that the radial AMB is only used at times when the rotor deviates from its equilibrium position and requires stabilization. As a consequence, T_b varies according to the bearing behavior. As long as $|T_\mathrm{b}| < |T_\mathrm{d}|$, the bearing will only decrease the rate of acceleration. However, as soon as $|T_\mathrm{b}| > |T_\mathrm{d}|$, the bearing causes a deceleration. This most likely occurs at high ratios of $B_\mathrm{b}/B_\mathrm{d}$ and high values of ω_r, at which the drive torque is decreased due to a decrease of ω_s, while the bearing torque is increased. Generally, the torque effect of the bearing is less significant if the bearing is required less often or with limited values of B_b, which illustrates the necessity for providing as much passive radial stability as possible in the motor *by design*. This is mainly achieved by the centering core, as displayed in Fig. 1(a), and its suitable dimensioning.

Two other torque components, aside from the ones given in Eqs. (6) and (7), exist due to the interaction of the magnetic dipole moment $\vec{m}_\mathrm{d}$ of the drive with the magnetic flux density $\vec{B}_\mathrm{b}$ of the bearing ($\vec{T}_\mathrm{bd}$) and vice versa of $\vec{m}_\mathrm{b}$ with $\vec{B}_\mathrm{d}$ ($\vec{T}_\mathrm{db}$). As the two vectors within the respective pairs rotate with different frequencies, the resulting torque components have zero average value and cause a pulsation of the torque with an angular frequency of ω_d. The components can be written as

$$\vec{T}_\mathrm{bd} = \vec{m}_\mathrm{d} \times \vec{B}_\mathrm{b} = B_\mathrm{b} \left[m_{\mathrm{d},x} \sin(\omega_\mathrm{d} t) - m_{\mathrm{d},y} \cos(\omega_\mathrm{d} t) \right] \vec{e}_z \tag{8}$$

and

$$\vec{T}_\mathrm{db} = \vec{m}_\mathrm{b} \times \vec{B}_\mathrm{d} = B_\mathrm{d} \left[m_{\mathrm{b},x} \sin(\omega_\mathrm{d} t) - m_{\mathrm{b},y} \cos(\omega_\mathrm{d} t) \right] \vec{e}_z. \tag{9}$$

Due to the respective slip angles, a phase shift of these torque components exists, which is accounted for in Eqs. (8) and (9) by the componentwise consideration of $\vec{m}_\mathrm{d}$ and $\vec{m}_\mathrm{b}$, respectively. The overall torque is calculated as $\vec{T} = \vec{T}_\mathrm{d} + \vec{T}_\mathrm{bd} + \vec{T}_\mathrm{db} + \vec{T}_\mathrm{b}$.

As B exhibits a gradient in the practical motor setup, as shown in Fig. 1(b), additional oscillating torque components will be acting on the rotor in case of a displacement from its equilibrium position at the center between the drive coils. The reason for this behavior is illustrated in Fig. 2(b), which shows that the magnitude of the magnetic flux density becomes increasingly dependent on the angle of $\vec{B}_\mathrm{d}$ the more the rotor is displaced. The magnitude is high for angles at which $\vec{B}_\mathrm{d}$ is directed towards one of the drive coils (located at 0°, 90°, 180°, and 270°), while it is low when $\vec{B}_\mathrm{d}$ points into a direction between two coils. This results in a deviation from the ideal circular shape of the trace inscribed by the tip of the flux density vector that can be observed if no displacement occurs ($r_0 = 0$). While only the fundamental frequency ω_d is present for $r_0 = 0$, a first harmonic component, oscillating with $2\omega_\mathrm{d}$, is present for $r_0 \neq 0$, which results in a torque ripple of frequency $2\omega_\mathrm{d}$ as well. This ripple also is present, if the rotor is displaced in a pure drive field. Its magnitude depends on the gradient of B_d in radial direction and is, therefore, determined by the setup of the stator. Besides this ripple, the rotor will also experience a small increase in the average torque, as the average magnetic flux density is higher in case of a displacement, due to the closer proximity of the rotor to the stator.

4. Verification through simulations

To verify the considerations as outlined above, transient 3D FEM simulations have been carried out using the motor setup shown in Fig. 1(a) as a model. Additionally, calculations using an analytical model of the flux density distribution in the motor have been carried out to validate the presented equations. In this model, the combined drive and bearing coils are approximated by ten concentric current loops each, for which the distribution of the B-field can be calculated analytically (e.g. Elliot 1993). A comparison of the magnitude distribution is displayed in Fig. 3, which shows a good agreement of the values as obtained analytically (a) and by simulations (b).

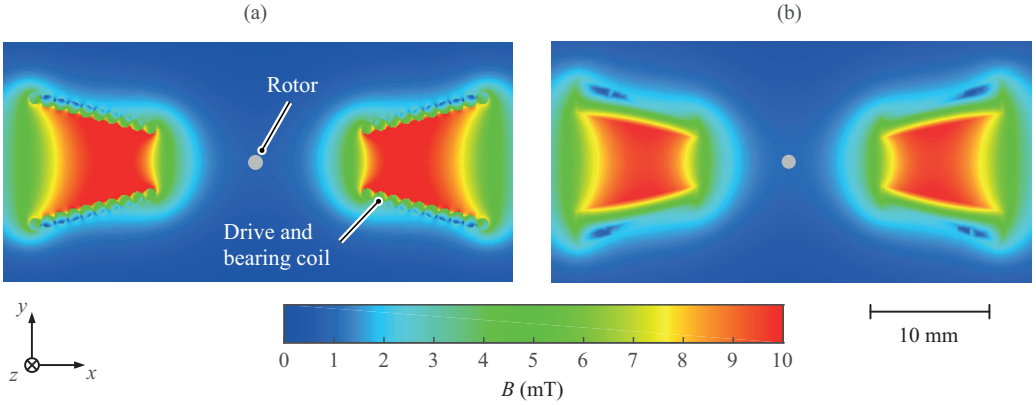

Fig. 3: Magnitude distribution of the magnetic flux density inside the motor as obtained by the analytical model (a) and by FEM electromagnetic simulations (b). The two coils along the x-axis have been used as an example and the instant at which the magnetic flux density vector $\vec{B}_\mathrm{d}$ points in the positive x direction is depicted. It can be seen that the results as obtained analytically and by simulations are in good agreement.

First, the sphere was placed in its equilibrium position ($r_0 = 0$) and the torques, as caused by a pure drive field $B = B_\mathrm{d}$ as well as a combined drive and radial bearing field $B = B_\mathrm{d} + B_\mathrm{b}$ with $B_\mathrm{b} = 0.5B_\mathrm{d}$, have been analytically calculated and simulated. The simulation parameters are listed in Table 1 and are identical to the conditions as shown in Fig. 1(b). The results for both cases are shown in Fig. 4(a), where a constant torque can be observed for a pure drive field, as expected. If a bearing field is added, the predicted oscillation of the torque around its equilibrium value with frequency ω_d occurs. This torque component originates from a combination of T_db and T_bd.

Second, a sphere which was displaced by $r_0 = 1$ mm from its equilibrium position has been considered in a pure drive field. The obtained results are shown in Fig. 4(b), which exhibits the oscillating component of the torque with a frequency of $2\omega_\mathrm{d}$ as predicted by the model. Moreover, the small increase in the average torque is visible and marked by ΔT. In all cases displayed in Fig. 4, a good agreement between analytically calculated and simulated results can be observed, validating the mathematical considerations as outlined in Section 3.

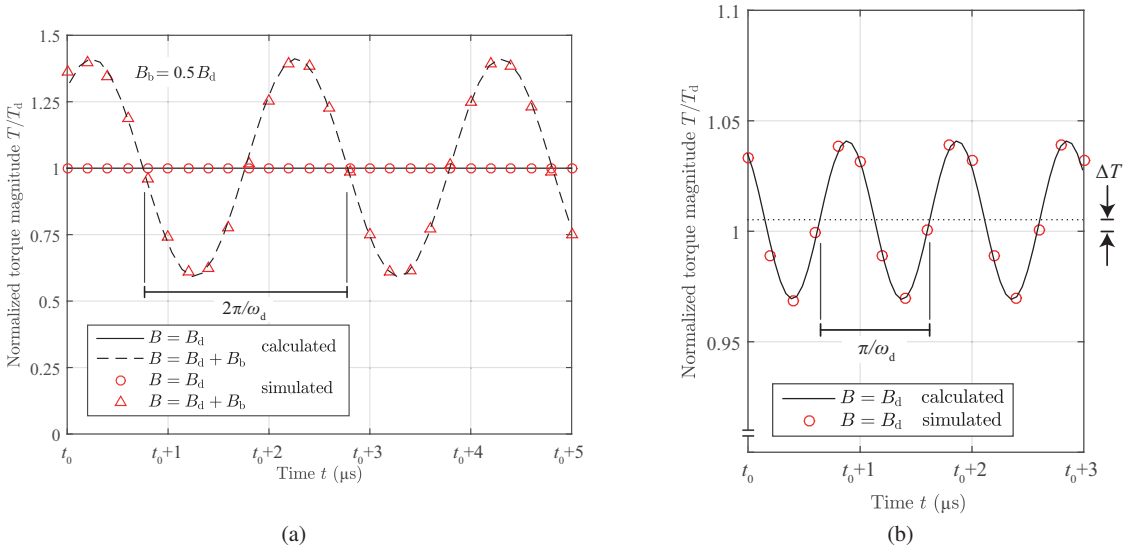

(a) (b)

Fig. 4: Time-dependent torque characteristics as obtained for a centered rotor ($r_0 = 0$) with the simulation parameters as listed in Table 1. A pure drive field as well as combined drive and bearing fields with $B_\mathrm{b} = 0.5B_\mathrm{d}$ have been used (a). Time-dependent torque characteristics for a rotor displaced by $r_0 = 1$ mm from its equilibrium position in a pure drive field (b). In both figures, the torque has been normalized to the constant value of T_d.

To provide guidelines for the relative dimensioning of the radial magnetic bearing with respect to the drive, the two torque components with non-zero average value, namely T_d and T_b, have been considered in more detail. Based on the ratio $B_\mathrm{b}/B_\mathrm{d}$ of the magnetic flux densities which cause these torques, it is possible to obtain the maximum achievable rotational speed. The latter is attained when the overall torque $T = 0$, corresponding to $|\vec{T}_\mathrm{b}| = |\vec{T}_\mathrm{d}|$. Based on Eqs. (6) and (7), the ratio

$$\epsilon = \frac{|\vec{T}_\mathrm{b}|}{|\vec{T}_\mathrm{d}|} = \frac{B_\mathrm{b} m_{\mathrm{b},y}}{B_\mathrm{d} m_{\mathrm{d},y}} = \left(\frac{B_\mathrm{b}}{B_\mathrm{d}}\right)^2 \cdot \frac{\frac{p}{\sqrt{\omega_\mathrm{d}-\omega_\mathrm{r}}} + \frac{\sqrt{\omega_\mathrm{d}-\omega_\mathrm{r}}}{p} + \sqrt{2}}{\frac{p}{\sqrt{\omega_\mathrm{r}}} + \frac{\sqrt{\omega_\mathrm{r}}}{p} + \sqrt{2}} \tag{10}$$

can be calculated, which has to be less than one for an acceleration of the rotor to be possible. By setting this ratio equal to one and solving for ω_r for a given ratio of $B_\mathrm{b}/B_\mathrm{d}$, the results as shown in Fig. 5 can be obtained. Different values of the drive frequency $f_\mathrm{d} = \omega_\mathrm{d}/2\pi$ have been considered. It can be seen that only above $B_\mathrm{b}/B_\mathrm{d} \approx 0.5$ a significant impact of B_b is visible, causing a decrease of the achievable synchronous rotational speed. This decrease is less significant for higher values of f_d. Generally, it should be noted that even for $B_\mathrm{b} = 0$, the synchronous rotational speed of n_syn is not attained in the practical motor setup, since other loss components, such as air friction, cannot be eliminated entirely.

The presented analyses show that a combined usage of the drive system and the radial AMB is possible and that, even for relatively high values of the bearing flux density, an accelerating torque can be obtained. The bearing has also been identified as the cause of different ripple components. However, these ripples do not contribute to the average value of the overall torque acting on the rotor.

Table 1: Simulation parameters

Rotor material	100Cr6
μ_r	≈ 4
σ	4.5 MS/m
a	0.5 mm
ω_d	500 kHz
ω_r	0

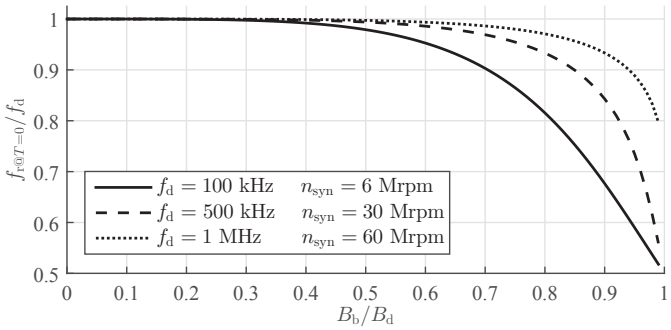

Fig. 5: Attainable mechanical rotational speed as a fraction of the synchronous speed (f_d) for varying ratios of the flux densities as gnerated by the bearing and drive. The considerations have been carried out for different values of f_d.

5. Conclusion

A verified analytical model for the torque interaction of the drive and radial AMB in an ultra-high speed spinning ball motor has been presented. Besides the identification of the occurring torque components, guidelines for assessing the maximum achievable rotational speed, dependent on the required flux density magnitude of the bearing, have been provided. The results facilitate the proper design of the radial AMB, which allows for stabilization of the rotor at rotational speeds beyond 20 Mrpm.

6. Acknowledgement

The authors would like to thank the Else & Friedrich Hugel Fund for Mechatronics for supporting this work.

References

Beams, J. W., Young, J. L., and Moore, J. W. (1946). "The Production of High Centrifugal Fields". In: *Journal of Applied Physics* 17.11, pp. 886–890.

Boletis, A. R. and Bleuler, H. (2002). "Achieving ultra-high rotating speeds". In: *Proceedings of the 8th International Symposium on Magnetic Bearings, Mito, Japan*, pp. 539–542.

Boletis, A. R. and Bleuler, H. (2004). "Three axis AMB high speed micro motor". In: *Proceedings of the 9th International Symposium on Magnetic Bearings, Lexington, Kentucky, USA*.

Elliot, Robert S. (1993). *Electromagnetics: history, theory, and applications*. IEEE.

Jackson, John (1999). *Classical electrodynamics*. New York: Wiley.

Reichert, T., Nussbaumer, T., and Kolar, J. W. (2012). "Complete analytical solution of electromagnetic field problem of high-speed spinning ball". In: *Journal of Applied Physics* 112.10, 104901.

Zwyssig, C., Kolar, J. W., and Round, S. D. (2009). "Megaspeed Drive Systems: Pushing Beyond 1 Million r/min". In: *IEEE/ASME Transactions on Mechatronics* 14.5, pp. 564–574.